
Ancient TL

www.ancienttl.org · ISSN: 2693-0935

Issue 24(1) - June 2006

<https://doi.org/10.26034/la.atl.v24.i1>

This issue is published under a Creative Commons Attribution 4.0 International (CC BY):

<https://creativecommons.org/licenses/by/4.0>



© Ancient TL, 2006

Spatial variation of dose rate from beta sources as measured using single grains

M. Ballarini¹, A.G. Wintle² and J. Wallinga¹

1. Netherlands Centre for Luminescence dating, Delft University of Technology, Mekelweg 15, NL-2629 JB Delft, The Netherlands (j.wallinga@tudelft.nl)

2. Institute of Geography and Earth Sciences, University of Wales, Aberystwyth, SY23 3DB, UK

(Received 3 February 2006; in final form 22 March 2006)

Abstract

Dose rates across the centre of a 9.7 mm diameter aluminium disc were measured using a 10 x 10 array of single grains of quartz held in holes drilled with 600 μm separation. The dose rates were obtained by measuring the OSL signals from quartz grains that previously had been given a known gamma dose and comparing them with those measured following increasing doses given by a beta source held 5 mm above the disc surface. The patterns of dose rate were obtained for four $^{90}\text{Sr}/^{90}\text{Y}$ beta sources. Two were found to produce a non-uniform dose rate at the disc surface, with one showing a factor of two across the 7.6 mm diameter of the area containing the 10 x 10 array. The implications for both single grain and multiple grain measurements are discussed.

Introduction

There has been an increasing number of publications relating to the use of Risø readers that have a special attachment for the measurement of the OSL signals from individual sand-sized grains using a focussed laser for optical stimulation (Duller and Murray, 2000). The main applications have been to the dating of sand related to archaeological sites (e.g. Jacobs et al., 2003), fluvial deposits (e.g. Thomas et al., 2005), glacial deposits (e.g. Glasser et al., 2006) and dosimetry studies of concrete blocks (Thomsen et al., 2003) and mortar (Jain et al., 2004). The prototype of Duller et al. (1999a; 1999b) used an 8 x 8 array of holes drilled into the surface of a 0.97 cm diameter aluminium disc. More recently a 9 x 9 array (Bøtter-Jensen et al., 2000) and then a 10 x 10 array (Bøtter-Jensen et al., 2003) have been used. The most commonly used discs have holes that are $\sim 300 \mu\text{m}$ in diameter and $300 \mu\text{m}$ deep with their centres being $600 \mu\text{m}$ apart; they are designed to receive single grains with diameters ranging from 180 to $250 \mu\text{m}$, a common size used in environmental and dosimetric studies.

The reproducibility of measurements made with the single grain system has been reported by Truscott et al. (2000) who used both $\text{Al}_2\text{O}_3:\text{C}$ grains and thermally annealed quartz grains. By making repeated measurements using the same dose, they demonstrated the precision and accuracy of the laser stimulation system. This resulted in a standard deviation of $\sim 3.5\%$ for repeated measurements. Thomsen et al. (2005) found similar results in another study of repeated paired measurements, though they noted that the standard deviation could be decreased by increasing the signal integration time; similar findings were reported by Jacobs et al. (2006).

The experiments described above have established the reproducibility of the measurement procedure. A crucial part of using such a system is calibration of the beta source. This can be undertaken using individual grains that have previously been sensitised and stabilised by heating, and then been given a known gamma dose. The SAR protocol (Murray and Wintle, 2000) can then be used to determine the dose rate. Measurements of such gamma-irradiated quartz, should provide a distribution of doses that has a standard deviation that is similar to that of the grains given repeated beta doses. However, it has been shown that the scatter in dose rate is much larger (Thomsen et al., 2005). Thomsen et al. (2005) also presented evidence that using individual dose rates for each grain position, rather than an average dose rate for the whole disc, caused a reduction in the error term. Their results indicated that for their source, non-uniformity of dose rate did not contribute more than about 5% to the variability observed. However, given the different methods of source construction, it is possible that other sources may be more variable, and that is what this paper explores.

Source	Activity	n	$R_1 < R_2 < R_3$	R_5/R_1	Recuperation (% of R_1)	Min.	Max.	Average dose rate
5583	74 MBq	600	4	30	4	1.81	3.39	2.66 ± 0.04 mGy/s
5626	24.1 MBq	1600	15	38	6	1.02	1.44	1.236 ± 0.003 mGy/s
6100	1.48 GBq	1200	1	15	1	0.064	0.142	0.103 ± 0.002 Gy/s
6088	1.48 GBq	2000	1	21	1	0.117	0.166	0.147 ± 0.002 Gy/s

Table 1: Sources used, source activity, number of grains (n) investigated, percentage of grains that fail a series of quality control tests (dose response curve, recycling ratio and recuperation), average minimum, maximum and average dose rate. R are normalized luminescence values (L/T) for cycles 1 to 5 in the SAR protocol. R_5/R_1 is the recycling ratio. $R_1 < R_2 < R_3$ indicated that the dose response curve grows systematically.

Although the grains are individually optically simulated with the laser, both irradiation and heating of all 100 grains on a disc is carried out simultaneously. The heating of the grains will be very similar as aluminium is a good conductor. The uniformity of irradiation will depend upon the source-sample distance and the homogeneity of the source. For older versions of the Risø TL/OSL reader, the source-sample distance is 7 mm, as reported by Mauz and Lang (2005). For more recent readers, this distance has been reduced to 5 mm (Bøtter-Jensen et al., 2000). It might be assumed that this geometry would provide uniform irradiation across the 7.6 mm diameter of the area occupied by the holes in the special single grain disc. However, this should not be assumed given recently reported spatial variations in dose rate reported when using a source with a ceramic substrate in a stand-alone irradiator with the sources at distances of 15 to 25 mm from a radioluminescent probe made of CaF_2 (Spooner and Allsop, 2000).

It is particularly important to take account of all laboratory-derived sources of error in the measurement of single grains before obtaining dose distributions for naturally-irradiated sand grains. Thus it is important to investigate the dose rate for each position across a single grain disc. In this study, we investigate the uniformity of the dose rate across a sample disc for discs irradiated in a Risø TL/OSL reader

Equipment

The Risø TL/OSL DA-15 reader employed in the study was purchased in 2002 and has a source-sample distance of 5 mm (Bøtter-Jensen et al., 2000). The carousel used to carry the sample discs has 48 positions. Single grain discs were placed on the carousel of the reader with alternate positions left empty in order to avoid cross-talk during irradiation (Markey et al., 1997; Bøtter-Jensen et al., 2000) and optical stimulation (Bray et al., 2002). The discs were

carefully aligned so that they were identically oriented.

Four $^{90}\text{Sr}/^{90}\text{Y}$ sources are assessed, one original SIP silver plaque type source and three, more recent, SIF ceramic-substrate type sources manufactured by AEA Technology (Germany). The relative merits of these different types of source have been discussed by Aitken (1985) and by Spooner and Allsop (2000). In particular, it was reported that the active area of the SIP source has a diameter of 12 mm, whereas the equivalent diameter for the SIF source is only 5 mm (Spooner and Allsop, 2000). The sources were moved to the single grain reader. Each source was mounted in turn in the rotating aluminium wheel, which is built into a lead castle to provide shielding (Markey et al., 1997). The laboratory code and nominal activity for each source is given in Table 1.

Experimental procedure

The sources were calibrated using two batches of quartz (grain size of 180-212 μm) that had received doses of 5.00 and 3.18 Gy, respectively, using a ^{137}Cs γ -source at the Risø National Laboratory. This quartz has been heat treated in the Risø National Laboratory and is used by them for beta source calibrations. For all the quartz grains used in this study an OSL signal could be measured. For source 5626, quartz with a calibration dose of 3.18 Gy was used; for the other sources, quartz with 5.00 Gy was used. A SAR protocol was applied using a 10 s preheat at 240°C prior to the OSL measurement that was made for 1 s at 125°C, and a cut heat to 220°C after the delivery of the test dose. L_i and T_i are derived from the initial OSL signal (0.1 s) minus a background estimated from the last part of the stimulation curve (0.2 s). The SAR protocol used three regenerative beta doses to build up the dose-response curve, with $R = L/T$.

The reliability of the protocol within a measurement was assessed through three checks. First, the dose-response curves were tested for consistency; i.e. that

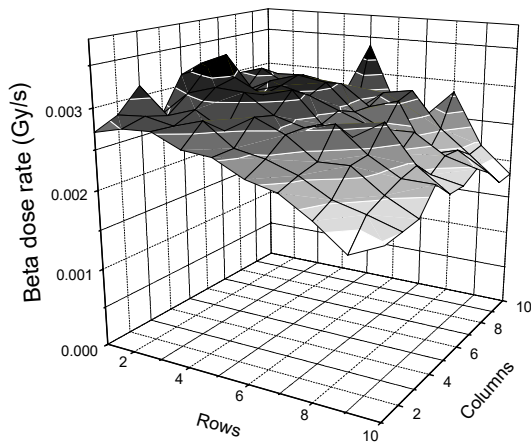


Figure 1: 3-D plot of dose rate (z axis) as a function of grain position (x, y) on ten-by-ten grid position for source 5583 (74 MBq SIP silver plaque source).

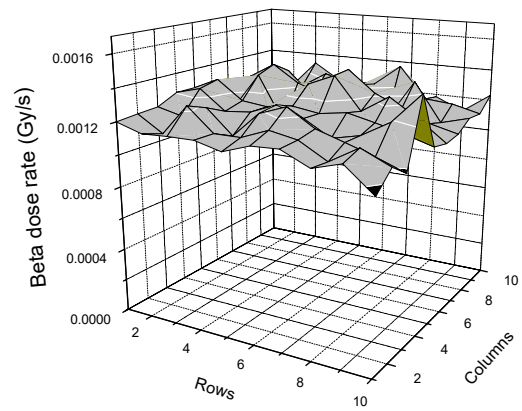


Figure 2: 3-D plot of dose rate (z axis) as a function of grain position (x, y) on ten-by-ten grid position for source 5626 (24.1 MBq SIF ceramic source).

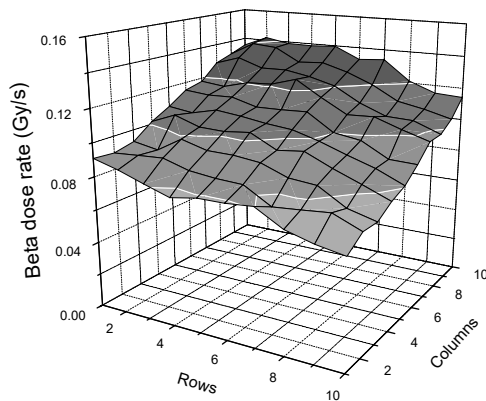


Figure 3: 3-D plot of dose rate (z axis) as a function of grain position (x, y) on ten-by-ten grid position for source 6100 (1.48 GBq SIF ceramic source).

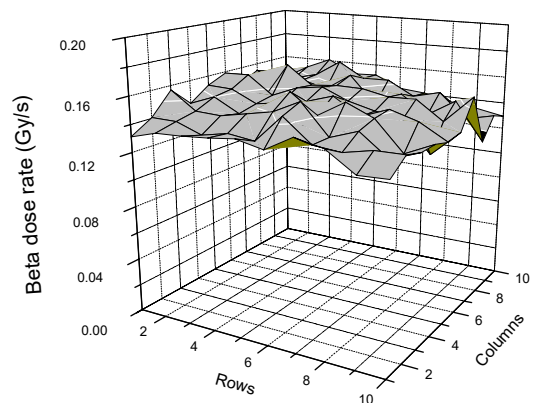


Figure 4: 3-D plot of dose rate (z axis) as a function of grain position (x, y) on ten-by-ten grid position for source 6088 (1.48 GBq SIF ceramic source).

larger doses gave larger OSL signals ($R1 < R2 < R3$). Second, the ratio ($R5/R1$) between the two sensitivity-corrected OSL responses generated from the same regenerative dose (recycling ratio) is within 10% of unity. Third, the OSL response when a zero regenerative dose is administered, expressed as a percentage of the corrected natural OSL signal L_n/T_n , is small (recuperation test of Murray and Wintle, 2000). The percentage of grains that failed the above checks, and thus were rejected, are listed in Table 1.

Results

The results of the experiment are plotted in 3-D graphs where on the x - and y -axis is the ten-by-ten

position-grid, and on the z -axis is the estimated dose rate. The spatial distributions of dose rates obtained using single-grain discs are shown in Figures 1-4. All four data sets have been rotated by about 90 degrees; this rotation was chosen for the best display of the plots for sources 5583 (Figure 1) and 6100 (Figure 3). The data used to obtain the plot shown in Figure 3 are given in Table 2. For this source (6100), 12 discs, each carrying 100 grains, were used. Each point in the table is obtained by calculating the mean and standard error (not shown) from the individual measurements. Table 3 gives the individual measurements (and the mean and standard error) for two grain positions (1, 10) and (10,2); these positions

	1	2	3	4	5	6	7	8	9	10
1	0.090	0.087	0.081	0.076	0.078	0.080	0.078	0.071	0.067	0.064
2	0.090	0.091	0.092	0.087	0.087	0.084	0.075	0.076	0.078	0.073
3	0.091	0.089	0.098	0.095	0.094	0.091	0.086	0.084	0.076	0.071
4	0.102	0.108	0.102	0.101	0.103	0.095	0.094	0.089	0.083	0.076
5	0.108	0.106	0.108	0.108	0.105	0.103	0.099	0.093	0.088	0.080
6	0.116	0.114	0.114	0.110	0.110	0.111	0.101	0.098	0.089	0.088
7	0.118	0.116	0.120	0.121	0.123	0.118	0.108	0.108	0.102	0.098
8	0.128	0.133	0.128	0.127	0.125	0.120	0.110	0.105	0.104	0.097
9	0.131	0.140	0.138	0.131	0.132	0.126	0.121	0.112	0.105	0.104
10	0.136	0.142	0.139	0.137	0.140	0.133	0.134	0.121	0.115	0.111

Table 2: Source 6100 - Average individual single-grain dose-rate estimates (Gy/s) calculated for each position on the disc (100 grains are measured on each of 12 discs). In bold are the minimum and maximum dose rate values.

Position	Individual dose rate estimates (Gy/s)								Mean and s.e.
(1,10)	0.136	0.147	0.142	0.132	0.149	0.150	0.137	0.142	0.142±0.002
(10,2)	0.065	0.060	0.071	0.060	0.054	0.060	0.063	0.085	0.064±0.003

Table 3: Source 6100 - Dose rate measurements for 8 discs for two positions

correspond to the positions giving the lowest and highest dose rates, respectively. In each case, the dose rate was measured on 8 grains (out of the possible 12 prior to the grain rejection criteria being applied).

For determination of the dose rate for one grain on one disc, e.g. that at position (1, 1) on the first disc, it is necessary to be sure that the OSL signal is measured reliably. The reproducibility of the OSL signal measurement through a SAR run can be assessed by looking at the recorded position of the laser beam during successive measurements. An example of this is shown in Figure 5, where for the first grain the position of the measurement of the gamma dose is shown at the centre of a circle drawn to represent the size of a 300 µm diameter hole. The co-ordinate centres for each subsequent beta dose measurement (irradiation with source 6100) are shown. There is a slight movement (<20 µm) for the second measurements and the remaining six are clustered at ~100 µm from the initial position. This shows that no further relative measurement has occurred as a result of the movement of the disc whilst in the reader.

The fact that the disc is not moving far, with respect to the coordinate system, implies that it is not moving

far relative to the beta source either. This will allow for the dose response curve for each grain in that position to be well defined. However, for it to be meaningful to calculate the mean dose rate for a grain position, the discs should be placed in a similar position relative to the source. That this has been accomplished in this study, can be seen by plotting the recorded co-ordinates for four consecutively measured discs. In Figure 6 these positions are shown for both the first measurement (i.e. related to the gamma dose) and the last measurement (i.e. related to the final beta dose). From this plot it is inferred that the dose rate is being measured at positions relative to the source that are within 500 µm.

Discussion

A source's homogeneity can be assessed by visual inspection of the 3-D plots. Flat surfaces indicate spatial homogeneity of irradiation and such a surface is found for sources 5626 and 6088. If a non-flat surface is observed, this indicates that irradiation does not occur uniformly, and these are found for sources 5583 and 6100. The results shown in Figures 1-4 indicate that two of the sources result in a steep gradient in the dose rate across the 10 x 10 array of grains. In Figure 1, showing the data obtained using the SIP type source (5583), the dose rate varies from 3.39 mGy/s to 1.81 mGy/s. In Figure 3, showing the

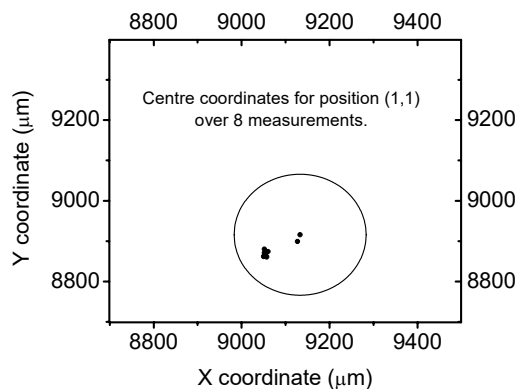


Figure 5: Plot of centre co-ordinates for position (1, 1) as obtained over 8 OSL measurements made in a SAR cycle. Circle drawn to show size of hole with its centre at the first measurement position.

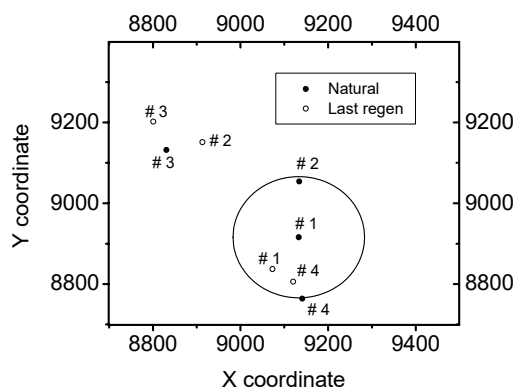


Figure 6: Plot of centre co-ordinates for first and last measurements of SAR run for position (1, 1) on each of four discs (#1, #2, #3 and #4). Circle drawn to show size of hole.

data obtained using the SIF type source 6100, the dose rate varies from 0.142 Gy/s to 0.064 Gy/s (Table 1). For the other two SIF type sources, 5626 (Figure 2) and 6088 (Figure 4), the dose rate is much more uniform, and the maximum and minimum values for each source are given in Table 1. The ratio of the maximum to minimum values for the latter two sources is 1.41.

Non-uniform irradiation could be caused by non-uniform distribution of radioactive material on the source face. The method of manufacture of both types of sources employs the dropping of a liquid

containing ^{90}Sr onto a surface. In the case of SIP sources, the liquid is evaporated from the silver plate that forms the front of the source (Aitken, 1985). In the manufacture of SIF sources, the liquid is dropped onto a ceramic surface, into which it can penetrate; this may result in it not being uniformly distributed prior to evaporation. There appears to be no immediate solution to this problem with source construction, though it has been suggested that a mini X-ray generator may provide an alternative (but uniform) irradiation source (Andersen et al., 2003).

An alternative interpretation of the results is that the steep gradient in dose rate for sources 5583 and 6100 is caused by a mis-alignment of the source and the aperture through which the electrons pass. This possibility is however not likely seeing the different orientations of the dose-rate gradients for the two sources. The experiment was not repeated with the sources in different orientations.

For single grain measurements, it is possible to obtain individual dose rates for each hole in a single grain disc and, indeed, it is essential to do this to avoid incorrect dose evaluation. However, it should be pointed out that there is likely to be a problem if these poorly-performing sources are used for measurement of aliquots made up of several thousand grains. It would still be possible to measure an average dose rate for a non-uniform source, using the uniformly bright calibration quartz spread over a 9 mm diameter area in the centre of the disc. However, in the case of un-sensitised sand-sized quartz grains, it has been demonstrated that only a small percentage of grains produce almost all the OSL signal (e.g. Duller et al., 2000; Jacobs et al., 2003). These bright grains would be randomly distributed amongst the thousand or so grains on a sample disc. The value of the equivalent dose that would be calculated would depend upon exactly where the bright grains were situated. For a non-uniform source such as 6100, this would result in a previously unconsidered source of scatter in the distribution of the values of the equivalent dose. In contrast to the case for single grains, it is not possible to obtain an appropriate calibration and this will result in meaningless D_e distributions or, at the very least, prevent using overdispersion measurements to obtain information on bleaching history. For laboratories without access to a single grain reader, or equipment of the type used by Spooner and Allsop (2000), a simple test can be applied. A quartz grain can be placed several mm from the centre of a regular sample disc and given a dose. The disc should then be rotated by 180° and the SAR protocol applied. If the number of seconds of irradiation required to match the first irradiation time

is identical, then the disc may be considered to be uniformly irradiated.

Conclusions

Using OSL signals from highly-sensitised quartz grains that had been given a laboratory gamma dose, we have demonstrated that two of the four $^{90}\text{Sr}/^{90}\text{Y}$ sources in the Netherlands Centre for Luminescence Dating in Delft give non-uniform dose rates across the inner area of a standard 9.7 mm diameter sample disc. The measurement used single grains mounted in a 10 x 10 array within an area of 7.6 mm diameter.

Of the two sources that resulted in a uniform dose rate, both were of the SIF type. Of the two sources that showed poor uniformity, one was of the SIP type and one of the SIF type. This study has shown that it is essential to make a calibration for each hole position when using the single grain facility. The gradient across the 7.6 mm diameter area would make it inappropriate for use in regular dosimetry measurements in which grains of variable sensitivity are randomly distributed across a 9 mm diameter area of the 9.7 mm diameter sample disc. Effects of the non-uniform dose rate on regular dosimetry measurements may be mitigated by mounting the sample only on the central area of the disc.

It is not clear whether the strong non-uniformity of the measured dose rate is the result of non-uniformity of the radioactive material on the source face or the mis-alignment of the source and the aperture, but the former is considered more likely.

Acknowledgements

We thank Shengua Li (University of Hong Kong, China) for reviewing the manuscript and Kristina Thomsen (Risø, Denmark) for commenting on an earlier version. This work is supported by the Netherlands Organisation for Scientific research (NWO) through grants 863.03.006 and 834.03.003.

References

- Aitken, M.J. (1985). *Thermoluminescence Dating*. Oxford University Press, Oxford.
- Andersen, C. E., Bøtter-Jensen, L. and Murray, A.S. (2003). A mini X-ray generator as an alternative to a Sr-90/Y-90 beta source in luminescence dating. *Radiation Measurements* **37**, 557-561.
- Bøtter-Jensen, L., Bulur, E., Duller, G.A.T. and Murray, A.S. (2000). Advances in luminescence instrument systems. *Radiation Measurements* **32**, 523-528.
- Bøtter-Jensen, L., Andersen, C. E., Duller, G.A.T. and Murray, A.S. (2003). Developments in radiation, stimulation and observation facilities in luminescence measurements. *Radiation Measurements* **37**, 535-541.
- Bray, H. E., Bailey, R.M. and Stokes, S. (2002). Quantification of cross-irradiation and cross-illumination using a Risø TL/OSL DA-15 reader. *Radiation Measurements* **35**, 275-280.
- Duller, G. A. T., Bøtter-Jensen, L., Murray, A.S. and Truscott, A.J. (1999a). Single grain laser luminescence (SGLL) measurements using a novel automated reader. *Nuclear Instruments and Methods in Physics Research B* **155**, 506-514.
- Duller, G.A.T., Bøtter-Jensen, L., Kohsiek, P. and Murray, A.S. (1999b). A high-sensitivity optically stimulated luminescence scanning system for measurement of single sand-sized grains. *Radiation Protection Dosimetry* **84**, 325-330.
- Duller, G. A. T., Bøtter-Jensen, L. and Murray, A.S. (2000). Optical dating of single sand-sized grains of quartz: sources of variability. *Radiation Measurements* **32**, 453-457.
- Duller, G. A. T. and Murray, A.S. (2000). Luminescence dating of sediments using individual mineral grains. *Geologos* **5**, 87-106.
- Glasser, N.F., Harrison, S., Ivy-Oches, S., Duller, G.A.T. and Kubik, P.W. (2006). Evidence from the Rio Bayo valley on the extent of the North Patagonian Icefield during the Late Pleistocene-Holocene transition. *Quaternary Research* **65**, 70-77.
- Jacobs, Z., Duller, G. A. T. and Wintle, A. G. (2003). Optical dating of dune sand from Blombos Cave, South Africa: II - single grain data. *Journal of Human Evolution* **44**, 613-625.
- Jacobs, Z., Duller, G. A. T. and Wintle, A. G. (2006). Interpretation of single grain De distributions and calculation of De. *Radiation Measurements* **41**, 264-277.
- Jain, M., Thomsen, K.J., Bøtter-Jensen, L. and Murray, A.S. (2004). Thermal transfer and apparent-dose distributions in poorly bleached mortar samples: results from single grains and small aliquots of quartz. *Radiation Measurements* **38**, 101-109.
- Markey, B.G., Bøtter-Jensen, L. and Duller, G.A.T. (1997). A new, flexible system for measuring thermally and optically stimulated luminescence. *Radiation Measurements* **27**, 83-89.
- Mauz, B. and Lang, A. (2005). The dose rate of beta sources for optical dating applications: a comparison between fine silt and fine sand quartz. *Ancient TL* **22**, 45-48.
- Murray, A. S. and Wintle, A.G. (2000). Luminescence dating of quartz using an improved single-aliquot regenerative-dose protocol. *Radiation Measurements* **32**, 57-73.

- Spooner, N. A. and Allsop, A. (2000). The spatial variation of dose-rate from Sr-90/Y-90 beta sources for use in luminescence dating. *Radiation Measurements* **32**, 49-56.
- Thomas, P. J., Jain, M., Juyal, N. and Singhvi, A.K. (2005). Comparison of single-grain and small-aliquot OSL dose estimates in <3000 years of river sediments from South India. *Radiation Measurements* **39**, 457-469.
- Thomsen, K. J., Jain, M., Bøtter-Jensen, L., Murray, A.S. and Jungner, H. (2003). Variation with depth of dose distributions in single grains of quartz extracted from an irradiated concrete block. *Radiation Measurements* **37**, 315-321.
- Thomsen, K. J., Murray, A.S. and Bøtter-Jensen, L. (2005). Sources of variability in OSL dose measurements using single grains of quartz. *Radiation Measurements* **39**, 47-61.
- Truscott, A. J., Duller, G.A.T., Bøtter-Jensen, L., Murray, A.S. and Wintle, A.G. (2000). Reproducibility of optically stimulated luminescence measurements from single grains of Al₂O₃:C and annealed quartz. *Radiation Measurements* **32**, 447-451.

Reviewer
Shenghua Li

Analysis of quartz LM-OSL curves

J.H. Choi^{1,2}, G.A.T. Duller² and A.G. Wintle²

1. Geochronology Team, Korea Basic Science Institute, Daejeon 305-333, South Korea

2. Institute of Geography and Earth Sciences, University of Wales, Aberystwyth, SY23 3DB, UK

(Received 22 December 2005; in final form 15 May 2006)

Abstract

Measurement of the optically stimulated luminescence signal during linear ramping of the stimulation power (LM-OSL) is a useful and efficient method for separating constituent OSL components, and for detailed investigation of the luminescence properties of each component. However, the practical procedures for the analysis of the quartz LM-OSL signal have been largely ambiguous in previous publications. In this study, we discuss various aspects of the analysis of quartz LM-OSL curves. This includes the measurement of background count rate, deconvolution of the LM-OSL curves using commercially available software, derivation of detrapping probabilities from the fitting results, and the identification and characterisation of each OSL component based upon the photoionisation cross-sections derived from these values.

Introduction

A decade ago, Bulur (1996) introduced an innovative method of measuring optically stimulated luminescence (OSL) which is now widely known as LM-OSL (Linearly Modulated OSL). The LM-OSL signal is observed by linearly increasing the stimulation power of the light source during measurement, and it has many advantages over continuous wave OSL (CW-OSL) measured with constant stimulation power. By ramping the stimulation power from zero to a particular value (usually the maximum power of the light source), the OSL signal appears as a series of peaks; each peak represents a component of the OSL signal with a particular physical parameter, namely the photoionisation cross-section. The LM-OSL signal allows more effective and accurate characterisation of each OSL component than the CW-OSL signal, and thus, LM-OSL can be used as an essential tool for understanding processes giving rise to OSL and improvement of the optical dating procedure based on measurement of CW-OSL.

Recently, various physical aspects of OSL components (such as sensitivity, dose response,

thermal stability, and recuperation) have been investigated using LM-OSL signals from single and multiple quartz grains (Bulur et al., 2000, 2002; Jain et al., 2003; Kuhns et al., 2000; Singarayer, 2002; Singarayer and Bailey, 2003). In addition, LM-OSL signals have been used to identify the cause of problems in dating sediments (equivalent dose estimation) using quartz grains (Choi et al., 2003a and b; Tsukamoto et al., 2003). Singarayer and Bailey (2003, 2004) showed that one of the slow components (the slowest component they observed) saturated at much higher doses (> 1000 Gy) than the fast component that usually dominates the initial part of the CW-OSL signal; this component has potential for dating old samples of around 1 Ma. All these studies make use of LM-OSL signals and require the separation and identification of the different OSL components; this can be achieved, in principle, by mathematical deconvolution of LM-OSL curves. However, the process of fitting components to the LM-OSL curve and the derivation of trap parameters for each component are somewhat ambiguous in the earlier publications.

In this paper, we present the process of fitting components to the LM-OSL curve obtained from multi-grain single aliquots of quartz, using commercially available software and the derivation of useful trap parameters from the fitting results. The procedures are applied to two sedimentary quartz samples that have very different LM-OSL characteristics.

Samples and experimental details

Quartz grains extracted from a fluvial sediment from the Kenyan Rift Valley (lab code ER4) and an aeolian dune sand from Tasmania, Australia (lab code TNE9517) were used in this study. The quartz fraction of 150-250 μm diameter grains was recovered by density separation and sieving, and purified through sequential use of 10 vols H_2O_2 , 10% HCl, and 40% HF. The detailed luminescence characteristics of these two samples have been

reported elsewhere (Choi et al., in press; Duller and Augustinus, in press).

Quartz OSL was measured using an automated luminescence measurement system (Risø TL/OSL-DA-15), which is equipped with a $^{90}\text{Sr}/^{90}\text{Y}$ beta source delivering $0.11 \text{ Gy}\cdot\text{s}^{-1}$ to the sample position. Quartz OSL was stimulated using blue LED arrays ($470 \pm 30 \text{ nm}$) with a green long-pass GG-420 filter in front of the LEDs, and the stimulation temperature was 125°C . Photon detection was by an EMI9235QA photomultiplier tube through 7.5 mm thickness of Hoya U-340 filter. Quartz LM-OSL signals were measured by linearly ramping the stimulation power of the blue-LEDs from 0 to 90 % ($\sim 30 \text{ mW}\cdot\text{cm}^{-2}$) of full power over a period of 3600 s with the photon counts being collected every 4 s. The quartz grains were mounted over an area of 8 mm diameter on 9.7 mm diameter aluminium discs using silicone oil (~ 1600 grains per aliquot).

Deconvolution of the LM-OSL curves was performed using commercial software SigmaPlotTM (ver. 7), which employs the Marquardt-Levenberg algorithm for linear and non-linear fitting.

Deconvolution of LM-OSL curves

Background subtraction and testing the linearity of the increase in stimulation power

Before fitting LM-OSL curves, it is important to consider the background count rate while ramping the stimulation power. In order to measure the background, 5 blank aluminium discs (coated with a thin silicone oil layer, but without quartz grains on top of it) were prepared and the photon count rate was measured whilst increasing the stimulation power of the blue LEDs from 0 to $30 \text{ mW}\cdot\text{cm}^{-2}$ for 3600 s (the disc was held at a constant temperature of 125°C). The background count rates from all the blank discs were found to be dependent upon the stimulation light intensity; the background count rates increased with increasing stimulation light intensity. The average of the background data from five aliquots is depicted as open circles in Fig. 1(a).

Two further experiments were performed under the same stimulation conditions. In the first, aluminium discs were used without silicone spray, and in the second, stainless-steel discs (with and without silicone spray) were used; similar data sets (not shown here) were obtained. Thus, it was concluded that the increase of the background count rate with increasing stimulation light intensity, as shown in Fig. 1(a), is the result of stimulation light breaking through the Hoya U-340 detection filter and arriving at the photomultiplier tube.

The point-by-point average of the background data could be best fitted using a quadratic function ($y = 294 + 0.04921 x + 0.00003239 x^2$, solid line in Fig. 1(a)) with an R^2 value of 0.998. If the background is solely related to the stimulation light, the intensity of which is increased linearly, the background should increase linearly. A possible explanation for the non-linearity is a slight change in wavelength of the LED emission as the power is increased, allowing more photons to pass through the Hoya U-340 filter, though this hypothesis has not been tested.

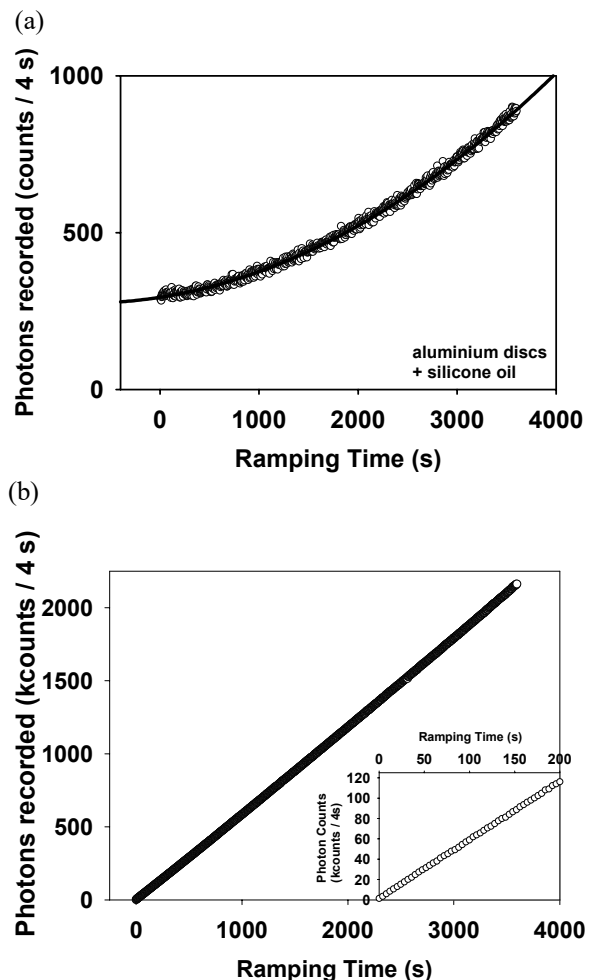


Figure 1: (a) Background count rate as measured on a blank disc (aluminium discs with silicone spray, but no quartz grains) with the standard U-340 filters. The average of the background data can be best fitted using a quadratic function. (b) Photon counts measured while ramping the blue LED power from 0 to 90% over a period of 3600s. For this measurement the U-340 filters were removed and replaced by an opaque disc with a pin hole and three neutral density filters. The inset shows the same data over the interval from 0 to 5% of full power in the first 200 s.

For subsequent LM-OSL measurements, we take the quadratic fit derived above as the background, and all the LM-OSL curve fittings described in this paper are performed after subtraction of this background from the measured data sets.

Another critical test to make prior to LM-OSL measurement is that the increase in the intensity of the light emitted by the blue LEDs is linear during the measurement. The mathematics described by Bulur (1996) is based upon the assumption that this is the case. This was tested by removing the U-340 filters and replacing them with an opaque disc in which a pin hole was placed. Three semi-silvered neutral density filters (ND3.0, ND1.0 and ND1.0) were then added to attenuate the signal by a factor of 100,000 so that the photomultiplier was not blinded. A blank aluminium disc was placed on the carousel. In this way, the photomultiplier could be used to directly measure the intensity of the blue LEDs during an LM-OSL procedure. Fig. 1(b) shows the photon counts measured during the 3600 s of an LM-OSL procedure in which the blue LEDs were ramped from 0 to 90% of full power. Fitting a straight line to this data gives an R^2 value of 0.9999. The inset to Fig. 1(b) shows that the increase is linear even over the range from 0 to 5% of full power. (Please note that caution is required when making this measurement to avoid blinding, and permanently damaging, the photomultiplier tube by exposing it to the blue LEDs without appropriate shielding).

Equations for use in SigmaPlot™

The LM-OSL curves were obtained by stimulating the natural quartz grains of samples TNE9517 and ER4 (one aliquot for each sample) with increasing stimulation light intensity from 0 to 30 mW·cm⁻² for 3600 s at 125°C. The photon count data sets were transferred to the graphics software (SigmaPlot™), the background subtracted and the LM-OSL vs. ramping time plots used for curve fitting (Fig 2). The simplest form of the equation governing the LM-OSL curve has been given in Bulur et al. (2002):

$$L(t) = n_0 b (t/P) \exp(-bt^2/2P) \quad (\text{Eqn. 1})$$

where $L(t)$ is the luminescence intensity as a function of time (t), n_0 is the number of trapped electrons, P is the total stimulation time, b is the detrapping probability, which is proportional to the photoionisation cross-section (σ) and the maximum stimulation light intensity (I_0) with $b = \sigma I_0$ (see Appendix 1 for example calculations).

The number of OSL components has been shown to vary from sample to sample; Jain et al. (2003)

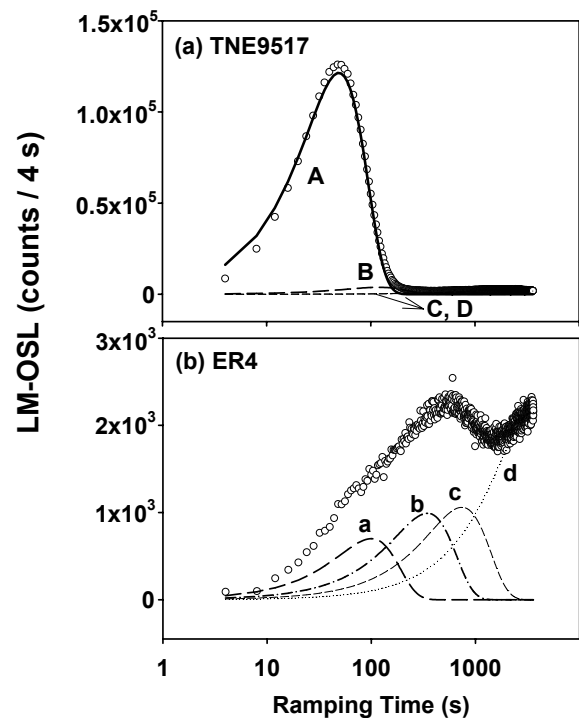


Figure 2: Separation of quartz LM-OSL signals by mathematical fitting with commercially available software (SigmaPlot™). Both (a) an aeolian sample from Tasmania (TNE9517) and (b) a fluvial sample from Kenya (ER4) could be separated into 4 components, but having a different selection of photoionisation cross-sections (Table 5).

identified 6 OSL components from 9 sedimentary quartz samples, but Singarayer and Bailey (2003) reported that most of the sedimentary quartz samples that they analysed had 5 components. Choi et al. (in press) also showed that more than 80% of the samples investigated in their study have 5 components, whereas they identified only 3 OSL components from the well-studied sedimentary quartz WIDG8 from western Australia. However, the number of components in these previous studies is based on the LM-OSL curves observed from multi-grain aliquots, whereas others have shown that the number of components varies from grain-to-grain when measurements are made on individual grains (Bulur et al., 2002; Yoshida et al., 2003).

Although the value of σ (cm²) is the fundamental property, b (s⁻¹) is more convenient for use in the software package. On the basis of Eqn. 1, the following form (Eqn. 2) was entered into the fitting program of the software ("Regression Wizard" in SigmaPlot™).

Relative σ		N = 3	b_N / b_1	N = 4	b_N / b_1	N = 5	b_N / b_1	N = 6	b_N / b_2
$\sigma_F / \sigma_F = 1.0$	n_1	9.988×10^6	1.0	9.870×10^6	1.0	5.212×10^6	1.0	6.967×10^1	1.2×10^5
	b_1	1.468		1.482		1.482		1.735×10^5	
$\sigma_M / \sigma_F = 0.2$	n_2	7.917×10^5	0.1	7.370×10^5	0.2	4.659×10^6	1.0	5.887×10^6	1.0
	b_2	0.1584		0.2580		1.482		1.482	
$\sigma_{S1} / \sigma_F = 0.06$	n_3	8.935×10^6	0.001	8.074×10^5	0.01	7.370×10^5	0.2	3.983×10^6	1.0
	b_3	0.0010		0.0107		0.2580		1.482	
$\sigma_{S2} / \sigma_F = 0.01$	n_4			9.118×10^6	0.001	8.074×10^5	0.01	7.370×10^5	0.2
	b_4			0.0008		0.0107		0.2580	
$\sigma_{S3} / \sigma_F = 0.001$	n_5					9.118×10^6	0.001	8.074×10^5	0.01
	b_5					0.0008		0.0107	
$\sigma_{S4} / \sigma_F = 0.0001$	n_6							9.118×10^6	0.001
	b_6							0.0008	
	R^2	0.999		0.999		0.999		0.999	

Notes:

Relative σ values are from Jain et al. (2003). N is the number of OSL components in the fitting equation (Eqn. 2). Initial b_N values for fitting were derived from Jain et al. (2003) (see text). Initial n_N was set to 10^5 and n_N and b_N were constrained to be $n_N > 0$, $b_N > 0$. The number of iterations, step size, and tolerance were set to 10^5 , 10^2 and 10^{-500} , respectively. Shaded boxes represent imaginary components with very high b and low n values (see text for details).

Table 1: Output parameters of LM-OSL curve fitting of sample TNE9517 with different numbers of OSL components (initial b values taken from Jain et al. (2003), listed in order of descending value)

$$f = n_1 b_1 (t/P) \exp(-b_1 t^2/2P) + n_2 b_2 (t/P) \exp(-b_2 t^2/2P) + n_3 b_3 (t/P) \exp(-b_3 t^2/2P) + n_4 b_4 (t/P) \exp(-b_4 t^2/2P) + n_5 b_5 (t/P) \exp(-b_5 t^2/2P) + \dots + n_N b_N (t/P) \exp(-b_N t^2/2P) \tag{Eqn. 2}$$

where P, the total stimulation time, was fixed as 3600 s in this experiment, and the values n_N (number of trapped electrons) and b_N (detrapping probability) are those obtained through mathematical fitting.

One way of seeing whether the individual values of b (and thus σ , since $b = \sigma I_0$) have the same relative behaviour as has been found by others, is to compare the ratios of the parameter b for each of the N components. These can also be compared with the relative values of σ published by others. We have chosen to compare our ratios of b values with the ratios for σ values of the components reported by Jain et al. (2003). The latter ratios can be seen in the furthest left column of Table 1. The data sets for TNE9517 and ER4 are available on the journal web page as described in Appendix 2.

Fitting LM-OSL curve for TNE9517

The LM-OSL curve for sample TNE9517 was fitted with a varying number of constituent OSL components (3, 4, 5 and 6 components; N = 3, 4, 5, 6 in Eqn. 2), and the results are summarised in Table 1.

The initial n_N values were set to be 100000 and the initial values for b_N were based on the values of σ given by Jain et al. (2003), but for a maximum power of $30 \text{ mW} \cdot \text{cm}^{-2}$, rather than $47 \text{ mW} \cdot \text{cm}^{-2}$ as used by Jain et al. (2003). For N=3 components, these were σ_F , σ_M and σ_{S1} for the fast, medium and slow1 components with initial values of 2.32×10^{-17} , 5.59×10^{-18} and $1.33 \times 10^{-18} \text{ (cm}^2\text{)}$, respectively, giving rise to b values of 1.65, 0.396, and $0.0943 \text{ (s}^{-1}\text{)}$. The value of P in Eqn. 2 was fixed as 3600 s, and the maximum number of iterations was 10^5 with a step size of 10^2 . The tolerance was set to 10^{-500} in order that the fitting process stops when the absolute value of the difference between the norm of the residual (square root of the sum of the squares of the residuals by definition), from one iteration to the next, is less than 10^{-500} . For N=4, 5 and 6, values of b were calculated from the data of Jain et al. (2003) giving 0.0147, 0.0015 and 0.0002 (s^{-1}) for slow2, slow3 and slow4.

From Table 1, it can be seen that the values of b_1 , b_2 and b_3 obtained when N was set to 3 are similar, but not identical, to the values entered at the start of the iteration. The ratios of b_2 / b_1 and b_3 / b_1 are similar to the equivalent ratios of σ_M / σ_F and σ_{S1} / σ_F , using the values of Jain et al. (2003). Fitting of 3 components was good as shown by the R^2 value being 0.999.

Similar results were obtained for N=4 when adding in the extra components (slow2 for N=4). The values of b_1 were very similar for N=3 and N=4, and those for b_2 and b_3 were not dissimilar. For N=5 (additionally adding in the b value for slow3), it can be seen from the repetition of 1.482 as both the calculated b_1 and b_2 values, and the simultaneous division of n between n_1 and n_2 , that the software has created two almost identical LM-OSL signal components. This implies redundancy in the number of components, and the conclusion is that only 4 components are present in the TNE9517 signal in Fig. 2(a). For N=6 (additionally adding in the b value for slow4) then the same redundancy is seen by the identical values found for b_2 and b_3 . In addition, for N=6, an imaginary component, with a very high value of b ($b_1 = 1.735 \times 10^5$) and a very low value of n ($n_1 = 6.967 \times 10^1$) can be seen (shaded box in Table 1). This result also confirms the conclusion reached for N=5, namely that TNE9517 LM-OSL is well represented by 4 components. Thus the signals are probably the fast, medium, slow2 and slow3. In addition, the relative values of b , shown as b_i / b_1 , are similar to the ratios for σ_i / σ_F for the photoionisation cross-sections of Jain et al. (2003).

Fitting LM-OSL curve for ER4

The same approach was taken for ER4 (Fig. 2(b)), starting by entering the values of b for the fast, medium and slow1 components for N=3. In this case, the fit was not good, with $R^2 = 0.841$, and the values obtained were not similar to those entered (Table 2). When fitting for N=4 (adding in b for slow2), the use of 4 components resulted in a better fit ($R^2 = 0.915$). However, N=5 (adding in b for slow3) resulted in a worse fit, owing to the calculation of 3 components with very high b values (shaded part of Table 2). For N=6, the 4 components found for N=4 were again calculated, together with two imaginary components that had no effect on the fitting ($R^2 = 0.915$, as for N=4). This again confirms that ER4 has 4 components, as previously suggested by Choi et al. (in press). In this case, the components are thought to be the medium, slow2, slow3 and slow4 components of Jain et al. (2003) on the basis of the ratios of the b values compared with the ratios of σ . In no calculation was a fast component identified.

Relative σ		N = 3	b_N / b_1	N = 4	b_N / b_1	N = 5	b_N / b_4	N = 6	b_N / b_3
$\sigma_M / \sigma_M = 1.0$	n_1	2.659×10^5		1.153×10^5		3.814×10^4		5.009×10^{-5}	
	b_1	0.1224	1.0	0.3607	1.0	1.832×10^6	1.2×10^8	6.159×10^8	1.7×10^9
$\sigma_{S1} / \sigma_M = 0.24$	n_2	1.478×10^6		5.647×10^5		1.615×10^{-7}		2.702×10^{-5}	
	b_2	0.0105	0.09	0.0302	0.08	4.014×10^4	2.6×10^6	1.138×10^5	3.2×10^5
$\sigma_{S2} / \sigma_M = 0.04$	n_3	1.084×10^7		1.292×10^6		3.072×10^4		1.153×10^5	
	b_3	0.0004	0.003	0.0066	0.02	3.409×10^3	2.2×10^5	0.3607	1.0
$\sigma_{S3} / \sigma_M = 0.004$	n_4			1.215×10^7		1.461×10^6		5.647×10^5	
	b_4			0.0003	0.0008	0.0155	1.0	0.0302	0.08
$\sigma_{S4} / \sigma_M = 0.0005$	n_5					9.920×10^6		1.292×10^6	
	b_5					0.0005	0.03	0.0066	0.02
	n_6							1.215×10^7	0.0008
	b_6							0.0003	
	R^2	0.841		0.915		0.402		0.915	

Notes

Relative σ values are from Jain et al. (2003). N is the number of OSL components in the fitting equation (Eqn. 2). Initial b_N values for fitting were derived from Jain et al. (2003) (see text). Initial n_N was set to 10^5 and n_N and b_N were constrained to be $n_N > 0$, $b_N > 0$. The number of iterations, step size, and tolerance were set to 10^5 , 10^2 and 10^{-500} , respectively. Shaded boxes represent imaginary components with very high b and low n values (see text for details).

Table 2: Output parameters of LM-OSL curve fitting of sample ER4 with different numbers of OSL components (initial b values starting from Jain et al. 's (2003) fast component b values)

Tests for the fitting of ER4 LM-OSL curve

Since no fast component was found, even though the initial estimate for the first b value (b_1) was given the value for the fast component of Jain et al. (2003), it was expected that the ability to fit components would not be sensitive to the selection of initial b values. In particular, we anticipated that starting with b_1 equal to the value of the medium component of Jain et al. (2003) would also result in the same 4 components. The results from this analysis are given in Table 3. Firstly with $N=3$, the results were identical to those calculated in Table 2, with the same low value of R^2 (0.841). Increasing the number of components in the same way (by adding in the next smallest value of b), the curve was poorly fitted, with $R^2 = 0.402$ for both $N=4$ and $N=5$ and with two or three imaginary components being presented (shaded boxes in Table 3). Thus it seemed impossible to recover more than 3 components or values of b , unlike the situation when starting the calculation with the fast component b value.

The data for ER4 were re-investigated for $N=3$ and $N=4$, but using the values obtained from Table 2 ($N=4$ or $N=6$ with $R^2 = 0.915$). For $N=3$, the values of b obtained for the 3 components were the same as

had been obtained in both Table 2 and Table 3, with $R^2 = 0.841$ (Table 4). For $N=4$, the same three components were obtained with $R^2 = 0.841$, but an additional, imaginary, component was calculated (shaded box). The calculation for $N=4$ was then repeated, but constraining b to lie between 0 and 2, noting that b for the fast component was calculated to be 1.468 (Table 1). Application of this constraint resulted in four b values being obtained, each of which was numerically identical to those obtained in Table 2.

The sensitivity of the fitting algorithm to the choice of the initial values for the fitted parameters was investigated for two synthetic LM-OSL data sets (Appendix 3) where the true values of b and n were known. This showed that while a wide range of initial values resulted in identical final values, there were certain combinations of initial parameters that did not result in the correct values being determined. In these cases, b values that were either very large ($>10^3$) or very small ($<10^{-6}$) were produced. Further work is required to understand the optimum choice of initial starting parameters.

Relative σ		N = 3	b_N / b_1	N = 4	b_N / b_3	N = 5	b_N / b_4
$\sigma_M / \sigma_M = 1.0$	n_1	2.659×10^5	1.0	2.675×10^4	1.6×10^8	1.621×10^{-5}	7.7×10^9
	b_1	0.1224		2.443×10^6		1.188×10^8	
$\sigma_{S1} / \sigma_M = 0.24$	n_2	1.478×10^6	0.09	1.160×10^4	1.9×10^5	9.507×10^{-4}	4.9×10^9
	b_2	0.0105		2.898×10^3		7.521×10^7	
$\sigma_{S2} / \sigma_M = 0.04$	n_3	1.084×10^7	0.003	1.461×10^6	1.0	5.100×10^{-4}	7.9×10^6
	b_3	0.0004		0.0155		1.219×10^5	
$\sigma_{S3} / \sigma_M = 0.004$	n_4			9.920×10^6	0.03	1.461×10^6	1.0
	b_4			0.0005		0.0155	
$\sigma_{S4} / \sigma_M = 0.0005$	n_5					9.920×10^6	0.03
	b_5					0.0005	
	n_6						
	b_6						
	R^2	0.841		0.402		0.402	

Notes

Relative σ values are from Jain et al. (2003). N is the number of OSL components in the fitting equation (Eqn. 2). Initial b_N values for fitting were derived from Jain et al. (2003) (see text). Initial n_N was set to 10^5 and n_N and b_N were constrained to be $n_N > 0$, $b_N > 0$. The number of iterations, step size, and tolerance were set to 10^5 , 10^2 and 10^{-500} , respectively. Shaded boxes represent imaginary components with very high b and low n values (see text for details).

Table 3: Output parameters of LM-OSL curve fitting of sample ER4 with different numbers of OSL components (initial b values starting from Jain et al.'s (2003) medium component b values)

	N = 3	N = 4	†N = 4 (0<b<2)
n ₁	2.659 × 10 ⁵	3.980 × 10 ⁻⁴	1.153 × 10 ⁵
b ₁	0.1224	4.358 × 10 ⁷	0.3607
n ₂	1.478 × 10 ⁶	2.659 × 10 ⁵	5.647 × 10 ⁵
b ₂	0.0105	0.1224	0.0302
n ₃	1.084 × 10 ⁷	1.478 × 10 ⁶	1.292 × 10 ⁶
b ₃	0.0004	0.0105	0.0066
n ₄		1.084 × 10 ⁷	1.215 × 10 ⁷
b ₄		0.0004	0.0003
R ²	0.841	0.841	0.915

† b values obtained by constraining b values to between 0 and 2 were identical to the initial b values used in the fitting process. Shaded boxes represent imaginary components with very high b and low n values (see text for details).

Table 4: Output parameters of LM-OSL curve fitting of sample ER4 with different numbers of OSL components (using previous best-fit b values as initial values; $b_1 = 0.3607$, $b_2 = 0.0302$, $b_3 = 0.0066$, $b_4 = 0.0003$, see Table 2 ($N = 4$))

components	TNE9517			components	ER4		
	b (s ⁻¹)	σ (cm ²)	*Relative σ		b (s ⁻¹)	σ (cm ²)	*Relative σ
A	1.4820	2.1 × 10 ⁻¹⁷	1.0	a	0.3607	5.1 × 10 ⁻¹⁸	1.0
B	0.2580	3.6 × 10 ⁻¹⁸	0.2	b	0.0302	4.3 × 10 ⁻¹⁹	0.08
C	0.0107	1.5 × 10 ⁻¹⁹	0.01	c	0.0066	9.3 × 10 ⁻²⁰	0.02
D	0.0008	1.1 × 10 ⁻²⁰	0.001	d	0.0003	4.2 × 10 ⁻²¹	0.0008

*Relative σ values were obtained by dividing each σ value with the σ values of components A and a for samples TNE9517 and ER4, respectively.

Table 5: Photoionisation cross-sections of the OSL components of sample TNE9517 and ER4

Identification of quartz OSL components in TNE9517 and ER4

The fitting results of the LM-OSL curves for samples TNE9517 (Table 1) and ER4 (Table 4) show the need for 4 OSL components in each case. Provisionally, the separated OSL components are designated as A, B, C, D components for TNE9517, and a, b, c, and d components for ER4, based on the order of appearance of each peak (Table 5 and Fig. 2). Components C and D in TNE9517 are so small that they are barely visible in Fig. 2(a). For ER4, the first three components (a, b, c) appear to have a similar height in the LM-OSL plot (Fig. 2(b)).

The A, B, C, and D components of sample TNE9517 (Fig. 2(a)) can be classified as the fast, medium, slow2, and slow3, components, respectively. Sample ER4 appears not to have either a fast or slow1 OSL component. Thus, components a, b, c and d in Fig.

2(b) can be identified as the medium, slow2, slow3 and slow4 components on the basis of their σ values (Table 5).

Conclusions

In analysing quartz LM-OSL signals, it is important to consider the background count rates during LM-OSL measurements and to ensure that the stimulation power does increase linearly. The background count rates in this study showed a quadratic increase with increasing stimulation power, which might be the result of the combination of the stimulation light breaking through the detection filter and a change in wavelength of the stimulation emission as the power is increased. Direct measurement of the intensity of the light emitted from the blue LEDs confirmed that the power increases linearly during an LM-OSL measurement.

After the subtraction of background count rates, the LM-OSL curves were separated into OSL components using a commercially available software package (SigmaPlot™). The detrapping probabilities were better suited to the mathematical fitting than the photoionisation cross-sections. For TNE9517, a sample with a strong fast component, trying to fit more than 4 components resulted initially in the splitting of the first component (for N=5) and then in the creation of an additional component with an unrealistically high *b* value (for N=6). Similar problems were encountered for ER4, for which there was no fast component. In this case, using certain initial estimates for the parameters, it was also found necessary to restrict the range of *b* to between 0 and 2. The detrapping probabilities were used to identify the constituent OSL components. By comparison with published photoionisation cross-sections (Jain et al., 2003), it was shown that the aeolian sample from Tasmania (TNE9517) consists of 4 OSL components (fast, medium, slow 2, and slow 3). The fluvial sample from Kenya (ER4) also has 4 OSL components (medium, slow2, slow3 and slow4), but does not have the fast component. Neither of the samples has a slow1 component.

Acknowledgements

We would like to thank Dr. Mayank Jain for constructive discussions in the early stages of our study, and Bert Roberts for improving the clarity of the paper. JHC was financially supported by a Korea Research Foundation Grant funded by the Korean Government (MOEHRD, Basic Research Promotion Fund, C00265: M01-2004-000-20041-0). GATD acknowledges the support of the NERC through grant NER/T/S/2002/00677.

Appendix 1. Calculation of photoionisation cross-section (σ)

The photoionisation cross-section (σ), which is related to the detrapping probability (*b*) and the maximum stimulation intensity (I_0) ($b = \sigma I_0$), is a useful parameter for defining the OSL component. While the value of *b* obtained for a sample will depend upon the maximum intensity of the stimulation light source, the photoionisation cross-section is independent of the measurement conditions. Many authors have reported the photoionisation cross-section of each OSL component obtained using various methods for their samples (Bøtter-Jensen et al., 2003, and references therein). Here, we briefly show the calculation of the photoionisation cross-section from the output

parameters (*n* and *b*) obtained through mathematical fitting.

The energy (*E*) of one photon is given by

$$E = h \nu \quad (\text{Eqn. 3})$$

where *h* is Planck's constant, $6.63 \times 10^{-34} \text{ J}\cdot\text{s} = 6.63 \times 10^{-34} \text{ W}\cdot\text{s}^2$, and ν is frequency (for light with wavelength (λ) of 470 nm, $\nu = 3 \times 10^8 / 470 \times 10^{-9} \text{ s}^{-1}$, with $\nu = c / \lambda$, where *c* is the speed of light). Thus, the energy of one photon produced by a blue-LED (470 nm) is calculated to be $4.23 \times 10^{-19} \text{ W}\cdot\text{s}$. Given that the maximum intensity of the blue-LED array used to measure the LM-OSL curve from samples TNE9517 and ER4 is $30 \text{ mW}\cdot\text{cm}^{-2}$, the number of photons per unit time per unit area is $7.1 \times 10^{16} \text{ s}^{-1}\cdot\text{cm}^{-2}$ ($= 0.03 \text{ W}\cdot\text{cm}^{-2} / 4.23 \times 10^{-19} \text{ W}\cdot\text{s}$). Then, the photoionisation cross-section, σ , can be obtained by dividing the detrapping probability (*b*) of each OSL component by the photon flux I_0 , i.e. by $7.1 \times 10^{16} \text{ s}^{-1}\cdot\text{cm}^{-2}$. The photoionisation cross-sections of each OSL component of samples TNE9517 and ER4 are shown in Table 5.

Appendix 2. Example data sets

So that the reader can try using SigmaPlot™ (ver.7) to deconvolute LM-OSL curves, we have provided the data sets used in this paper. The LM-OSL data for TNE9517 and ER4, after background subtraction, are available as supplementary data from the Ancient TL website (<http://www.aber.ac.uk/ancient-tl>).

We suggest that you, like us, start with a large number of trapped electrons (*n*) in each of the traps. So, if you are investigating whether 3 components (N=3) are appropriate, enter $n_1 = 10^5$, $n_2 = 10^5$, and $n_3 = 10^5$. You could equally well try $n = 10^3$, $n = 10^5$, or $n = 10^7$.

For the maximum number of possible iterations, we used 10^5 , but you could equally well use a smaller number, e.g. 10^4 . The suggested step size is 10^2 . The suggested tolerance is 10^{-500} , as discussed in the text.

As a starting point for our measurements taken using blue ($\lambda = 470 \pm 30 \text{ nm}$) diode stimulation, the *b* values for each of the N components are taken as those derived from the photoionisation cross-sections (σ) of Jain et al. (2003). *b* is related to σ through $b = \sigma I_0$ as detailed in Appendix 1; I_0 is the photon flux for the maximum blue diode stimulation power used to collect the data. Values of *b* are 1.65, 0.3963, 0.0943, 0.0147, 0.0015 and 0.0002 (s^{-1}) for the fast, medium, slow 1, slow 2, slow 3 and slow 4 components, respectively.

Jain et al. (2003)			Singarayer and Bailey (2003)		
Component	σ cm ²	Relative σ	Component	σ cm ²	Relative σ
Ultrafast	2.9×10^{-16}	13	Ultrafast	7.0×10^{-16}	28
Fast	$(2.32 \pm 0.16) \times 10^{-17}$	1	Fast	$(2.5 \pm 0.3) \times 10^{-17}$	1
Medium	$(5.59 \pm 0.44) \times 10^{-18}$	0.2	Medium	$(5.9 \pm 2.0) \times 10^{-18}$	0.2
Slow 1	$(1.33 \pm 0.26) \times 10^{-18}$	0.06	S ₁	$(2.1 \pm 0.5) \times 10^{-19}$	0.01
Slow 2	$(2.08 \pm 0.46) \times 10^{-19}$	0.01	S ₂	$(1.2 \pm 0.2) \times 10^{-20}$	0.001
Slow 3	$(2.06 \pm 0.16) \times 10^{-20}$	0.001	S ₃	$(1.9 \pm 2.9) \times 10^{-21}$	0.0001
Slow 4	$(2.76 \pm 0.17) \times 10^{-21}$	0.0001			

Table A.1 : Comparison of published values of σ and the notation used by Jain et al. (2003) and Singarayer and Bailey (2003)

The same approach can be applied to the deconvolution of any LM-OSL data sets. For measurements made using other stimulation power and/or other stimulation wavelength, different values of b will be relevant. For stimulation sources with the same effective wavelength but different powers, the ratio b_M/b_F etc. will be constant. However, the ratio is dependent upon the wavelength, as shown by Singarayer and Bailey (2004).

It should also be remembered that there are two proposed notations for OSL trap identification beyond the fast and medium components, as proposed independently by Singarayer and Bailey (2003) and Jain et al. (2003) on the basis of their LM-OSL measurements on different sedimentary quartz samples. A comparative study of their notation and their values of σ are reproduced in Table A.1. In this paper we have adopted the notation of Jain et al. (2003).

Appendix 3. Synthetic LM-OSL data sets

Two additional example data sets are provided and are also available from the Ancient TL website (<http://www.aber.ac.uk/ancient-tl>). These are synthetic LM-OSL data where the values of b and n are known, and thus one can assess whether these parameters can be accurately recovered using the fitting procedure proposed in this paper.

Example 1 (Fig. A.1a) is an LM-OSL data set dominated by the fast component; the n and b values were set to have 93.6% fast, 4.9% medium, 0.8% slow 1, 0.4% slow 2, 0.2% slow 3 and 0.1% slow 4 components in the initial 0.8 s of the CW-OSL signal (Table A.2). Example 2 (Fig. A.1b) is an LM-OSL data set dominated by medium and slow components; the n and b values were set to have 3.3% fast, 34.7% medium, 7.8% slow 1, 41.3% slow 2, 9.5% slow 3

and 3.4% slow 4 components in the initial 0.8 s of the CW-OSL signal (Table A.3). Also shown in Tables A.2 and A.3 are the results of fitting these data sets using SigmaPlot™ (ver. 7) as described in this paper. In each case, the values of b and n are recovered accurately.

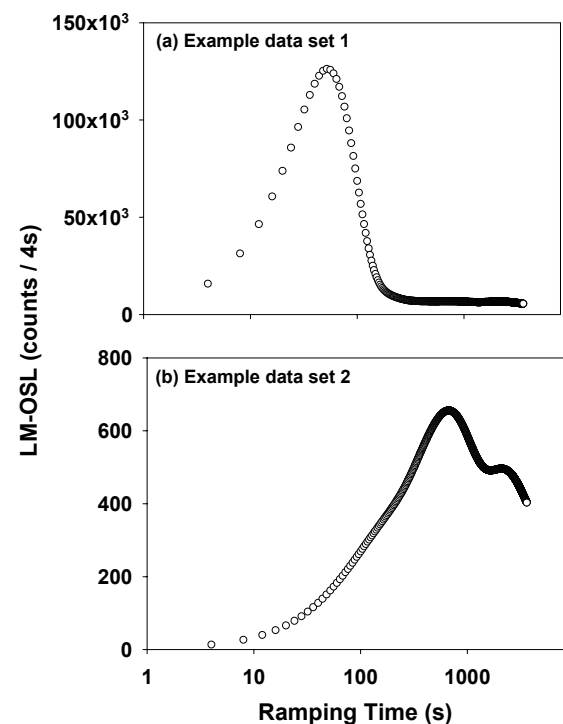


Fig. A.1: Synthetic LM-OSL data sets used for testing mathematical fitting using SigmaPlot™. (a) Example data set 1 is dominated (93.6%) by the fast component, and (b) Example data set 2 is dominated by the medium (34.7%) and slow2 (41.3%) components. Details of the parameters used to define these curves are given in Tables A.2 and A.3

In Table A.4, we tested several sets of initial values for fitting the synthetic data sets. In cases 1-4 (n_1 - n_6 were set to 10^5), all the parameters of Example data sets 1 and 2 were successfully recovered, regardless of the initial b values tested. However, in cases 5-8 (n_1 - n_6 were set to 10^3), the input parameters of Examples 1 and 2 could only be recovered when the initial b values were 1 or 0.1. This is rather counter intuitive since the fitting routine is able to fit the data accurately when unrealistic initial starting values of b are used, but not when the initial starting values of b are very similar to the true values. As was found for

the analysis of ER4, constraining the values of b to $0 < b < 2$ solves this problem, and allows the correct values to be recovered. Further work is required to understand the cause for this, but it does suggest that researchers should be aware of this problem if their analyses generate values of b very different from those which are expected from previously published literature. In such a situation, the analysis should be repeated using a range of initial parameters to test how robust such a conclusion is, and the values of b constrained to realistic values.

OSL component	Input parameters		Proportion (%)	Initial parameters		Output parameters (recovered)	
	n_0	b		n_0	b	n_0	b
Fast	9.98×10^6	1.3705	93.6	10^5	1.65	9.98×10^6 $\pm 4.60 \times 10^{-4}$	1.371 $\pm 4.13 \times 10^{-11}$
Medium	1.49×10^6	0.3302	4.9	10^5	0.3963	1.49×10^6 $\pm 6.19 \times 10^{-4}$	0.3302 $\pm 2.08 \times 10^{-10}$
Slow 1	9.45×10^5	0.0786	0.8	10^5	0.0943	9.45×10^5 $\pm 6.39 \times 10^{-4}$	0.0786 $\pm 9.59 \times 10^{-11}$
Slow 2	3.12×10^6	0.0123	0.4	10^5	0.0147	3.12×10^6 $\pm 1.25 \times 10^{-3}$	0.0123 $\pm 6.85 \times 10^{-12}$
Slow 3	1.13×10^7	0.00122	0.2	10^5	0.0015	1.13×10^7 $\pm 1.03 \times 10^{-1}$	0.00122 $\pm 5.40 \times 10^{-12}$
Slow 4	3.25×10^7	0.000163	0.1	10^5	0.0002	3.25×10^7 $\pm 4.58 \times 10^{-1}$	0.000163 $\pm 4.52 \times 10^{-12}$

Table A.2: Example data set 1 (Modelled LM-OSL data set dominated by fast component). The columns labelled "Input Parameters" show the values of n and b used to generate the modelled LM-OSL data set. Also given are the initial parameters used for fitting the data in SigmaPlotTM, and the values of n and b output from SigmaPlotTM.

OSL component	Input parameters		Proportion (%)	Initial parameters		Output parameters (recovered)	
	n_0	b		n_0	b	n_0	b
Fast	4.50×10^2	1.3705	3.3	10^5	1.65	4.50×10^2 $\pm 4.41 \times 10^{-5}$	1.371 $\pm 8.79 \times 10^{-8}$
Medium	1.34×10^4	0.3302	34.7	10^5	0.3963	1.34×10^4 $\pm 5.93 \times 10^{-5}$	0.3302 $\pm 2.22 \times 10^{-9}$
Slow 1	1.14×10^4	0.0786	7.8	10^5	0.0943	1.14×10^4 $\pm 6.12 \times 10^{-5}$	0.0786 $\pm 7.62 \times 10^{-10}$
Slow 2	3.78×10^5	0.0123	41.3	10^5	0.0147	3.78×10^5 $\pm 1.19 \times 10^{-4}$	0.0123 $\pm 5.43 \times 10^{-12}$
Slow 3	8.70×10^5	0.00122	9.5	10^5	0.0015	8.70×10^5 $\pm 9.88 \times 10^{-3}$	0.00122 $\pm 6.72 \times 10^{-12}$
Slow 4	2.34×10^6	0.000163	3.4	10^5	0.0002	2.34×10^6 $\pm 4.39 \times 10^{-2}$	0.000163 $\pm 6.01 \times 10^{-12}$

Table A.3: Example data set 2 (Modelled LM-OSL data set dominated by medium and slow components). The columns labelled "Input Parameters" show the values of n and b used to generate the modelled LM-OSL data set. Also given are the initial parameters used for fitting the data in SigmaPlotTM, and the values of n and b output from SigmaPlotTM.

	$n_1-n_6 = 10^5$				$n_1-n_6 = 10^3$			
	Case 1	Case 2	Case 3	Case 4	Case 5	Case 6	Case 7	Case 8
b_1	1.65	1.65	1	0.1	1.65	1.65	1	0.1
b_2	0.3963	0.40	1	0.1	0.3963	0.40	1	0.1
b_3	0.0943	0.09	1	0.1	0.0943	0.09	1	0.1
b_4	0.0147	0.01	1	0.1	0.0147	0.01	1	0.1
b_5	0.0015	0.002	1	0.1	0.0015	0.002	1	0.1
b_6	0.0002	0.0002	1	0.1	0.0002	0.0002	1	0.1
I [†]	○	○	○	○	×	×	○	○
II [†]	○	○	○	○	×	×	○	○

† I and II represent Example data sets 1 and 2, respectively.

○ Indicates that the b and n values used to define the synthetic data sets could be recovered.

× Indicates that the b and n values used to define the synthetic data sets could not be recovered.

Table A.4: Tests of the ability to recover the known b and n values for Example data sets 1 and 2. Eight different cases were tested, each with a different set of initial parameters used with SigmaPlot™.

References

- Bøtter-Jensen, L., McKeever, S.W.S., Wintle, A.G. (2003) *Optically Stimulated Luminescence Dosimetry*. Elsevier Science, Amsterdam, 355 pp.
- Bulur, E. (1996) An alternative technique for optically stimulated luminescence (OSL) experiment. *Radiation Measurements* **26**, 701-709.
- Bulur, E., Duller, G.A.T., Solongo, S., Bøtter-Jensen, L., Murray, A.S. (2002) LM-OSL from single grains of quartz: a preliminary study. *Radiation Measurements* **35**, 79-85.
- Bulur, E., Bøtter-Jensen, L., Murray, A.S. (2000) Optically stimulated luminescence from quartz measured using the linear modulation technique. *Radiation Measurements* **32**, 407-411.
- Choi, J.H., Murray, A.S., Jain, M., Cheong, C.S., Chang, H.W. (2003a) Luminescence dating of well-sorted marine terrace sediments on the southeastern coast of Korea. *Quaternary Science Reviews* **22**, 407-421.
- Choi, J.H., Murray, A.S., Cheong, C.S., Hong, D.G., Chang, H.W. (2003b) The resolution of stratigraphic inconsistency in the luminescence ages of marine terrace sediments from Korea. *Quaternary Science Reviews* **22**, 1201-1206.
- Choi, J.H., Duller, G.A.T., Wintle, A.G., Cheong, C.S. (in press) Luminescence characteristics of quartz from the southern Kenyan Rift Valley: Dose estimation using LM-OSL SAR. *Radiation Measurements*
- Duller, G.A.T., Augustinus, P.C. (in press) Reassessment of the record of linear dune activity in Tasmania using optical dating. *Quaternary Science Reviews*
- Jain, M., Murray, A.S., Bøtter-Jensen, L. (2003) Characterisation of blue-light stimulated luminescence components in different quartz samples: implications for dose measurement. *Radiation Measurements* **37**, 441-449.
- Kuhns, C.K., Agersnap Larsen, N., McKeever, S.W.S. (2000) Characteristics of LM-OSL from several different types of quartz. *Radiation Measurements* **32**, 413-418.
- Singarayer, J.S. (2002) *Linearly modulated optically stimulated luminescence of sedimentary quartz: physical mechanisms and implications for dating*. Unpublished D.Phil. thesis, University of Oxford.
- Singarayer, J.S., Bailey, R.M. (2003) Further investigations of the quartz optically stimulated luminescence components using linear modulation. *Radiation Measurements* **37**, 451-458.
- Singarayer, J.S., Bailey, R.M. (2004) Component-resolved bleaching spectra of quartz optically stimulated luminescence: preliminary results and implications for dating. *Radiation Measurements* **38**, 111-118.
- Tsukamoto, S., Rink, W.J., Watanuki, T. (2003) OSL of tephric loess and volcanic quartz in Japan and an alternative procedure for estimating D_e from a

fast OSL component. *Radiation Measurements* **37**, 459-465.

Yoshida, H., Roberts, R.G., Olley, J.M. (2003) Progress towards single-grain optical dating of fossil mud-wasp nests and associated rock art in northern Australia. *Quaternary Science Reviews* **22**, 1273-1278.

Reviewer

R.G. Roberts

Comments

This is a welcome addition to the luminescence literature, lifting the veil on the practicalities and potential pitfalls of mathematically separating LM-OSL components in quartz. The authors point out several interesting (and unexpected) features of LM-OSL analysis using commercially available software, and highlight the non-routine aspects of this form of data analysis. If LM-OSL signal-separation is to become more widely used as a means of characterising quartz samples or dating them using specific components, then the computational and statistical aspects of LM-OSL analysis need to be placed on a solid footing. This paper begins this process and should stimulate discussion about alternative and improved procedures for teasing apart the different LM-OSL components in quartz and other minerals.

An effective and reusable sampling pipe for luminescence dating

H.N. Chandel, A.D. Patel, H.R. Vaghela and G.P. Ubale

Machine Workshop, Physical Research Laboratory, Ahmedabad 380 009, India

(Received 10 February 2006; in final form 10 April 2006)

We present here a design of a simple to fabricate, and reusable, sampling pipe for luminescence dating (Figure 1, overleaf). This design effectively meets the needs of, 1) being rugged, 2) being reusable, 3) being easy to use in difficult terrains, 4) being light tight and 4) being moisture tight. The basic design involves the use of an aluminium or galvanized iron pipe sharpened at one end so as to provide easy penetration in the sediment. The second end is sealed with a stepped mild steel stub with a rivet pin so as to provide sufficient strength for pushing the pipe in the sediment with a geological hammer. The cap is made of aluminium and has two important design features. Firstly, it has an internal neoprene o-ring seal that remains in contact with the outer-side of the sampling pipe and ensures a perfect moisture seal. Secondly, the sharp edge of the sampling tube exactly meets the inner side of the cap, ensuring that the sample does not move during transit. The design of the cap is such that it push-fits on the sampling pipe, and hence allows the sample to be sealed almost instantaneously. This implies minimal user discomfort under a dark cloth, particularly under hot environments and on cliffs with minimal space for work. The luminescence laboratory at this institution has used these pipes effectively and has been satisfied. We will however welcome suggestions for further improvements.

Reviewer

Geoff Duller

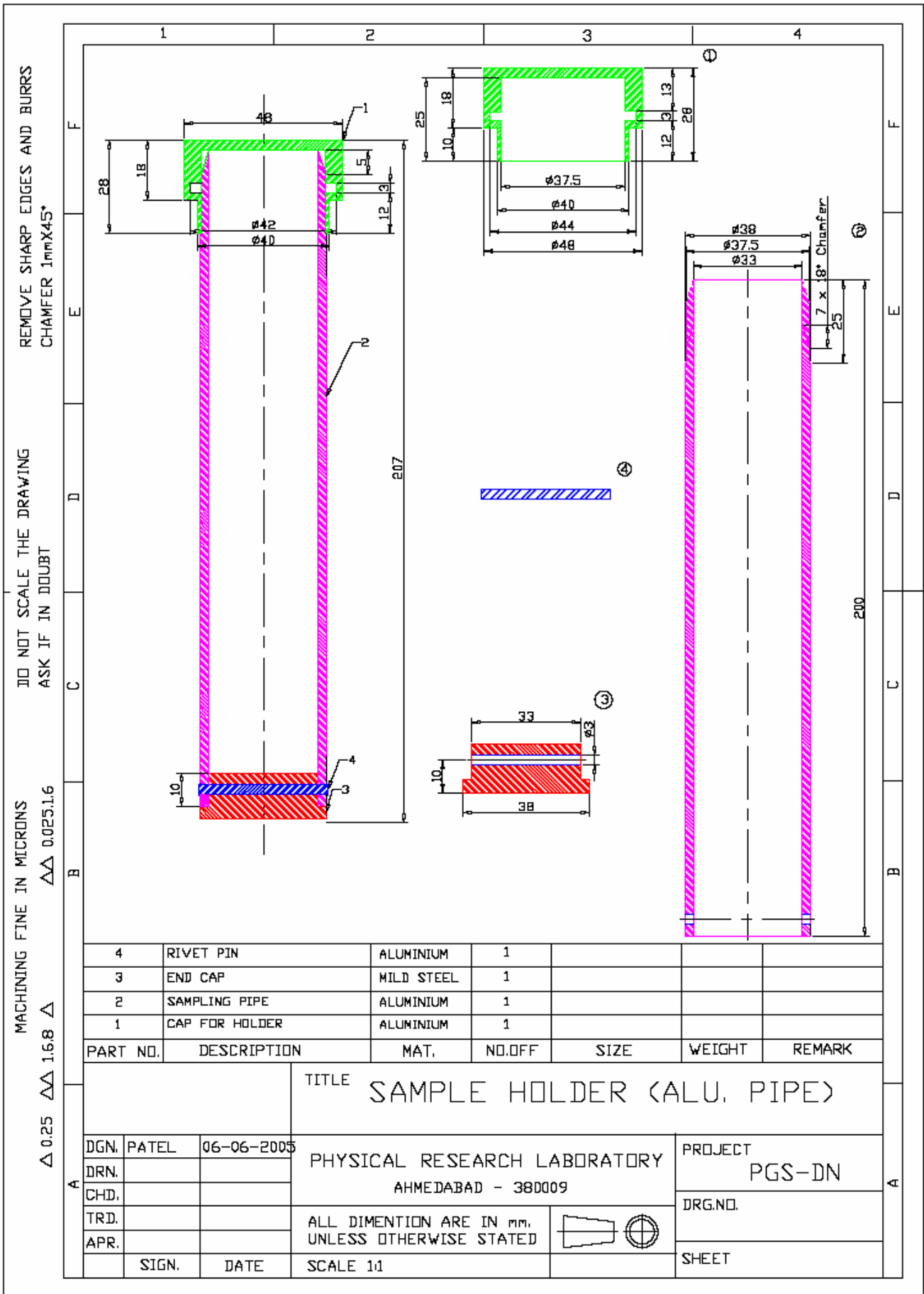


Figure 1: Plans for sample holder

Thesis Abstract

Author: Sara Ante
Thesis Title: Luminescence dating tests of detrital grains from sediment traps, Andvord Bay and Brialmont Cove, Antarctic Peninsula
Grade: MSc
Date: December 2005
Supervisor: Glenn Berger
Address: University of Nevada-Reno, Department of Geological Sciences and Engineering, United States of America, and Desert Research Institute, Reno (Berger)

D_E values ranged between 11.1 ± 0.7 ka and 31.4 ± 3.4 ka ($D_E = 21 - 58$ Gy), depending on season and depth of deposition. This indicates that these glacial marine sediments were unevenly and poorly bleached at deposition. Variations in luminescence traits between seasons and with trap depth may, however, be helpful for studying sedimentation processes in these fjords. Double-SAR experiments also resulted in anomalously high D_E values. SAR data for one sediment trap sample did exhibit characteristics predicted by Bailey et al.'s (2003) $D_E(t)$ model for poorly bleached sediments. Microprobe analyses did not reveal any significant differences in mineralogy between seasons and depth that would affect apparent age results.

Difficulties (e.g., large, diverse, erratic reservoir corrections) with radiocarbon dating have prompted photonic dating tests on Antarctic glacial marine sediments. This technique (clock zeroing is based on the last exposure to daylight of quartz and feldspar grains) was applied to modern-age sediments collected in two well-characterized fjords on the western side of the Antarctic Peninsula. Our deployed sediment traps collected approximately 14 months of deposition between January 2002 and March 2003. We conducted a series of multi-aliquot infrared-stimulated luminescence (IRSL) tests on polymineral silt-sized grains to evaluate the extent of the clock-zeroing process in this setting, to provide a foundation for applications elsewhere in the region. Comparisons were made between samples on the basis of seasonal differences and trap depth. Several double single-aliquot-regenerative (SAR) dose experiments were also performed on one of the sediment trap samples. Sediments representing summer and winter deposition were also characterized by microprobe analyses.

Had the sediments been exposed to sufficient sunlight at deposition, sediment grains collected by these traps would exhibit very low equivalent-dose (D_E) values. However, single and multi-aliquot experiments resulted in high (and variable) D_E values for both Andvord Bay and Brialmont Cove, which yield erroneously old ages, rather than zero. IRSL experiments have resulted in apparent ages for Andvord Bay ranging between 19.8 ± 1.4 ka and 56.8 ± 5.4 ka ($D_E = 48 - 123$ Gy), while Brialmont Cove

Bibliography

Compiled by Ann Wintle

From 1st January 2006 to 30th May 2006

- Anderson, A., Roberts, R., Dickinson, W., Clark, G., Burley, D., de Biran, A., Hope, G., and Nunn, P. (2006). Times of sand: Sedimentary history and archaeology at the Sigatoka Dunes, Fiji. *Geoarchaeology* **21**, 131-154.
- Antonioli, F., Kershaw, S., Renda, P., Rust, D., Belluomini, G., Cerasoli, M., Radtke, U., and Silenzi, S. (2006). Elevation of the last interglacial highstand in Sicily (Italy): A benchmark of coastal tectonics. *Quaternary International* **145**, 3-18.
- Beerten, K., and Stesmans, A. (2006). Some properties of Ti-related paramagnetic centres relevant for electron spin resonance dating of single sedimentary quartz grains. *Applied Radiation and Isotopes* **64**, 594-602.
- Beerten, K., and Stesmans, A. (2006). The use of Ti centers for estimating burial doses of single quartz grains: A case study from an aeolian deposit similar to 2 Ma old. *Radiation Measurements* **41**, 418-424.
- Boenigk, W., and Frechen, M. (2006). The Pliocene and Quaternary fluvial archives of the Rhine system. *Quaternary Science Reviews* **25**, 550-574.
- Bortolin, E., Bustos Griffin, E., Cruz-Zaragoza, E., Coste, V., and Onori, S. (2006). Electron paramagnetic resonance detection of Mexican irradiated spices. *International Journal of Food Science and Technology* **41**, 375-382.
- Brauer, A., Tempelhoff, K., and Murray, A. S. (2005). OSL-dating of fine-grained sand deposits and its implications for glacial stratigraphy and landscape evolution: research results from Stolzenhagen, northeastern Brandenburg. *Die Erde* **136**, 15-35.
- Brook, G. A., Srivastava, P., and Marais, E. (2006). Characteristics and OSL minimum ages of relict fluvial deposits near Sossus Vlei, Tsauhab River, Namibia, and a regional climate record for the last 30 ka. *Journal of Quaternary Science* **21**, 347-362.
- Carobene, L., Cirrincione, R., De Rosa, R., Gueli, A. M., Marino, S., and Troja, S. O. (2006). Thermal (TL) and optical stimulated luminescence (OSL) techniques for dating Quaternary colluvial volcanoclastic sediments: An example from the Crati Basin (Northern Calabria). *Quaternary International* **148**, 149-164.
- Carr, A. S., Thomas, D. S. G., and Bateman, M. D. (2006). Climatic and sea level controls on Late Quaternary eolian activity on the Agulhas Plain, South Africa. *Quaternary Research* **65**, 252-263.
- Chen, R., Pagonis, V., and Lawless, J. L. (2006). The nonmonotonic dose dependence of optically stimulated luminescence in Al₂O₃ : C: Analytical and numerical simulation results. *Journal of Applied Physics* **99**. Art. No. 033511
- Clarke, M. L., and Rendell, H. M. (2006). Effects of storminess, sand supply and the North Atlantic Oscillation on sand invasion and coastal dune accretion in western Portugal. *The Holocene* **16**, 341-355.
- Correcher, V., Garcia-Guinea, J., and Valle-Fuentes, F. J. (2006). Preliminary study of the thermally stimulated blue luminescence of ulexite. *Journal of Thermal Analysis and Calorimetry* **83**, 439-444.
- Couapel, M. J. J., and Bowles, C. J. (2006). Impact of gamma densitometry on the luminescence signal of quartz grains. *Geo-Marine Letters* **26**, 1-5.
- Coutard, S., Lautridou, J. P., Rhodes, E., and Clet, M. (2006). Tectonic, eustatic and climatic significance of raised beaches of Val de Saire, Cotentin, Normandy, France. *Quaternary Science Reviews* **25**, 595-611.

- Duffield, W., Riggs, N., Kaufman, D., Champion, D., Fenton, C., Forman, S., McIntosh, W., Hereford, R., Plescia, J., and Ort, M. (2006). Multiple constraints on the age of a Pleistocene lava dam across the Little Colorado River at Grand Falls, Arizona. *Geological Society of America Bulletin* **118**, 421-429.
- Eitel, B., Kadereit, A., Blümel, W.-D., Hüser, K., Lomax, J., and Hilgers, A. (2006). Environmental changes at the eastern Namib Desert margin before and after the Last Glacial Maximum: New evidence from fluvial deposits in the upper Hoanob River catchment, northwestern Namibia. *Palaeogeography, Palaeoclimatology, Palaeoecology* **234**, 201-222.
- Engin, B., Aydas, C., and Demirtas, H. (2006). ESR dosimetric properties of window glass. *Nuclear Instruments & Methods in Physics Research B* **243**, 149-155.
- Engin, B., Kapan-Yesilyurt, S., Taner, G., Demirtas, H., and Eken, M. (2006). ESR dating of Soma (Manisa, West Anatolia - Turkey) fossil gastropoda shells. *Nuclear Instruments & Methods in Physics Research B* **243**, 397-406.
- Falguères, C., Bahain, J. J., Pérez-González, A., Mercier, N., Santonja, M., and Dolo, J. M. (2006). The Lower Acheulian site of Ambrona, Soria (Spain): ages derived from a combined ESR/U-series model. *Journal of Archaeological Science* **33**, 149-157.
- Federici, P. R., and Pappalardo, M. (2006). Evidence of Marine Isotope Stage 5.5 highstand in Liguria (Italy) and its tectonic significance. *Quaternary International* **145**, 68-77.
- Gartia, R. K., Ranita, U., and Singh, T. B. (2006). Mathematical modeling of glow peaks of fluorites relevant to dosimetry and dating. *Indian Journal of Physics and Proceedings of the Indian Association for the Cultivation of Science* **80**, 181-185.
- Glasser, N. F., Harrison, S., Ivy-Ochs, S., Duller, G. A. T., and Kubik, P. W. (2006). Evidence from the Rio Bayo valley on the extent of the North Patagonian Icefield during the Late Pleistocene-Holocene transition. *Quaternary Research* **65**, 70-77.
- González, S., Huddart, D., Bennett, M. R., and González-Huesca, A. (2006). Human footprints in Central Mexico older than 40,000 years. *Quaternary Science Reviews* **25**, 201-222.
- Greenbaum, N., Porat, N., Rhodes, E., and Enzel, Y. (2006). Large floods during late Oxygen Isotope Stage 3, southern Negev desert, Israel. *Quaternary Science Reviews* **25**, 704-719.
- Grün, R., Maroto, J., Eggins, S., Stringer, C., Robertson, S., Taylor, L., Mortimer, G., and McCulloch, M. (2006). ESR and U-series analyses of enamel and dentine fragments of the Banyoles mandible. *Journal of Human Evolution* **50**, 347-358.
- Hebenstreit, R., Bose, M., and Murray, A. (2006). Late Pleistocene and early Holocene glaciations in Taiwanese mountains. *Quaternary International* **147**, 76-88.
- Huntley, D. J. (2006). An explanation of the power-law decay of luminescence. *Journal of Physics C* **18**, 1359-1365.
- Huntsman-Mapila, P., Ringrose, S., Mackay, A. W., Downey, W. S., Modisi, M., Coetzee, S. H., Tiercelin, J. J., Kampunzu, A. B., and Vanderpost, C. (2006). Use of the geochemical and biological sedimentary record in establishing palaeo-environments and climate change in the Lake Ngami basin, NW Botswana. *Quaternary International* **148**, 51-64.
- Ishida, Y., Ninagawa, K., Sakamoto, K., Toyoda, S., Nishido, H., and Gucsik, A. (2005). Thermoluminescence study of shocked sandstone. *Meteoritics & Planetary Science* **40**, A74-A74.
- Kinoshita, A., Figuty, L., and Baffa, O. (2006). Electron spin resonance dating of shells from the Sambaqui (Shell Mound) Capelinha, Sao Paulo, Brazil. *Brazilian Journal of Physics* **36**, 93-96.
- Kitagawa, Y., Imoto, H., Saito, M., Kurihara, H., Fujie, K., Toyoda, S., and Naruse, T. (2005). Mineral composition of clay fractions and oxygen vacancies in silt-sized quartz in soils on the Ka-Etsu plateau, Fukui, Central Japan -

Possibility of eolian dust brought from Northern Asia as parent material of soils. *Soil Science and Plant Nutrition* **51**, 999-1010.

Kitis, G., Chen, R., Pagonis, V., Carinou, E., Ascounis, P., and Kamenopoulou, V. (2006). Thermoluminescence under an exponential heating function: II Glow-curve deconvolution of experimental glow-curves. *Journal of Physics D* **39**, 1508-1514.

Kitis, G., Chen, R., Pagonis, V., Carinou, E., and Kamenopoulou, V. (2006). Thermoluminescence under an exponential heating function: I Theory. *Journal of Physics D* **39**, 1500-1507.

Kitis, G., and Furetta, C. (2005). Simulation of competing irradiation and fading effects in thermoluminescence dosimetry. *Radiation Effects and Defects in Solids* **160**, 285-296.

Koike, K., Nakagawa, M., Koike, C., Chihara, H., Okada, M., Matsumura, M., Awata, T., Atobe, K., and Takada, J. (2006). Properties of simulated cosmic matters after gamma-ray and neutron irradiation. *Planetary and Space Science* **54**, 325-330.

Koshchug, D. G., Gazeev, V. M., Gurbanov, A. G., Shabalin, R. V., and Vyatkin, S. V. (2005). EPR dating and evolution of the Elbrus volcano. *Applied Magnetic Resonance* **28**, 331-342.

Koul, D. K. (2006). Role of alkali ions in limiting the capacity of the 110 degrees C peak of quartz to remember the firing temperature. *Applied Radiation and Isotopes* **64**, 110-115.

Krauss, S. L., He, T. H., Lamont, B. B., Miller, B. P., and Enright, N. J. (2006). Late Quaternary climate change and spatial genetic structure in the shrub *Banksia hookeriana*. *Molecular Ecology* **15**, 1125-1137.

Kundu, H. K., Sato, H., Ganas, A., and Ikeya, M. (2005). ESR studies on calcite encrustation on Fili neotectonic fault, Greece. *Applied Magnetic Resonance* **29**, 185-194.

Kuster, Y., Hetzel, R., Krbetschek, M., and Tao, M. X. (2006). Holocene loess sedimentation along the Qilian Shan (China): significance for understanding the processes and timing of loess deposition. *Quaternary Science Reviews* **25**, 114-125.

Li, S. H., and Sun, J. M. (2006). Optical dating of Holocene dune sands from the Hulun Buir Desert, northeastern China. *The Holocene* **16**, 457-462.

Lindén, M., Möller, P., Björck, S., and Sandgren, P. (2006). Holocene shore displacement and deglaciation chronology in Norrbotten, Sweden. *Boreas* **35**, 1-22.

Litchfield, N. J., and Rieser, U. (2005). Optically stimulated luminescence age constraints for fluvial aggradation terraces and loess in the eastern North Island, New Zealand. *New Zealand Journal of Geology and Geophysics* **48**, 581-589.

Lutoev, V. P. (2005). Application of the ESR method in geological correlation problems. *Applied Magnetic Resonance* **28**, 311-330.

Mauz, B., Hilger, W., Muller, M. J., Zöller, L., and Dikau, R. (2005). Aeolian activity in Schleswig-Holstein (Germany): Landscape response to Late Glacial climate change and Holocene human impact. *Zeitschrift Fur Geomorphologie* **49**, 417-431.

Morwood, M. J., Brown, P., Jatmiko, T., Sutikna, E., Saptomo, W., Westaway, K. E., Due, R. A., Roberts, R. G., Maeda, T., Wasisto, S., and Djubianono, T. (2005). Further evidence for small-bodied hominins from the Late Pleistocene of Flores, Indonesia. *Nature* **437**, 1012-1017.

Nakamura, N., Cullings, H. M., Kodama, Y., Wada, T., Miyazawa, C., Lee, K., and Awa, A. A. (2006). A method to differentiate between the levels of ESR signals induced by sunlight and by ionizing radiation in teeth from atomic bomb survivors. *Radiation Research* **165**, 359-364.

- Ogundare, F. O., Balogun, F. A., Olowofela, J. A., Mokobia, C. E., and Fasunwon, O. O. (2006). Thermoluminescence characteristics of natural dolerite. *Nuclear Instruments & Methods in Physics Research B* **243**, 156-160.
- Pan, B. T., Wang, J. P., Gao, H. S., Chen, Y. Y., Li, J. J., and Liu, X. F. (2005). Terrace dating as an archive of the run-through of the Sanmen Gorges. *Progress in Natural Science* **15**, 1096-1103.
- Polymeris, G. S., Tsirliganis, N., Loukou, Z., and Kitis, G. (2006). A comparative study of the anomalous fading effects of TL and OSL signals of Durango apatite. *Physica Status Solidi a-Applications and Materials Science* **203**, 578-590.
- Ponnusamy, V., Ramasamy, V., and Anandalakshmi, K. (2006). Effect of preheating in biogenic shells - Thermostimulated luminescence and FTIR study. *Indian Journal of Pure & Applied Physics* **44**, 13-19.
- Przegietka, K. R., Richter, D., Chruscinska, A., Oczkowski, H. L., Lankauf, K. R., Szmanda, J., Luc, M., and Chudziak, A. (2005). Quartz luminescence applied in palaeoenvironmental reconstruction of a dune. *Physica Scripta* **T118**, 257-260.
- Radtke, U., and Schellmann, G. (2006). Uplift history along the Clermont Nose Traverse on the West Coast of Barbados during the last 500,000 years - Implications for paleo-sea level reconstructions. *Journal of Coastal Research* **22**, 350-360.
- Rasheedy, M. S. (2005). Method of Hoogenstraaten as a tool for obtaining the trap parameters of general-order thermoluminescence glow peaks. *Radiation Effects and Defects in Solids* **160**, 383-390.
- Rasheedy, M. S., and Zahran, E. M. (2006). The effect of the heating rate on the characteristics of some experimental thermoluminescence glow curves. *Physica Scripta* **73**, 98-102.
- Raukas, A., and Stankowski, W. (2005). Influence of sedimentological composition on OSL dating of glaciofluvial deposits: examples from Estonia. *Geological Quarterly* **49**, 463-470.
- Sun, J. M., Li, S. H., Han, P., and Chen, Y. Y. (2006). Holocene environmental changes in the central Inner Mongolia, based on single-aliquot-quartz optical dating and multi-proxy study of dune sands. *Palaeogeography Palaeoclimatology Palaeoecology* **233**, 51-62.
- Switzer, A. D., Bristow, C. S., and Jones, B. G. (2006). Investigation of large-scale washover of a small barrier system on the southeast Australian coast using ground penetrating radar. *Sedimentary Geology* **183**, 145-156.
- Takeda, K., and Ninagawa, K. (2005). Cathodoluminescence and thermoluminescence studies of Cr chondrites. *Meteoritics & Planetary Science* **40**, A150-A150.
- Tribolo, C., Mercier, N., Selo, M., Valladas, H., Joron, J.-L., Reyss, J.-L., Henshilwood, C., Sealy, J., and Yates, R. (2006). TL dating of burnt lithics from Blombos cave (South Africa): further evidence for the antiquity of modern human behaviour. *Archaeometry* **48**, 341-357.
- Vaille, J. R., Ravotti, F., Garcia, P., Glaser, M., Matias, S., Idri, K., Boch, J., Lorfevre, E., McNulty, P. J., Saigne, E., and Dusseau, L. (2005). Online dosimetry based on optically stimulated luminescence materials. *IEEE Transactions on Nuclear Science* **52**, 2578-2582.
- Veronese, I., Giussani, A., and Göksu, H. Y. (2006). Limits of thermoluminescence dosimetry using quartz extracted from recent building materials in urban settlements. *Journal of Environmental Radioactivity* **86**, 319-336.
- Wadley, L. (2005). A typological study of the final Middle Stone Age stone tools from Sibudu Cave, KwaZulu-Natal. *South African Archaeological Bulletin* **60**, 51-63.
- Ward, I. A. K., Fullagar, R. L. K., Boer-Mah, T., Head, L. M., Tacon, P. S. C., and Mulvaney, K. (2006). Comparison of sedimentation and occupation histories inside and outside rock shelters, Keep-River region, northwestern Australia. *Geoarchaeology* **21**, 1-27.

Webb, S., Cupper, M. L., and Robins, R. (2006). Pleistocene human footprints from the Willandra Lakes, southeastern Australia. *Journal of Human Evolution* **50**, 405-413.

Wintle, A. G., and Murray, A. S. (2006). A review of quartz optically stimulated luminescence characteristics and their relevance in single-aliquot regeneration dating protocols. *Radiation Measurements* **41**, 369-391.

Wolfe, S. A., Ollerhead, J., Huntley, D. J., and Lian, O. B. (2006). Holocene dune activity and environmental change in the prairie parkland and boreal forest, central Saskatchewan, Canada. *The Holocene* **16**, 17-29.

Woodroffe, C. D., Kennedy, D. M., Brooke, B. P., and Dickson, M. E. (2006). Geomorphological evolution of Lord Howe Island and carbonate production at the latitudinal limit to reef growth. *Journal of Coastal Research* **22**, 188-201.

Zacharias, N., Michael, C., Philaniotou-Hadjlanastasiou, O., Hein, A., and Bassiakos, Y. (2006). Fine-grain TL dating of archaeometallurgical furnace walls. *Journal of Cultural Heritage* **7**, 23-29.

Zhao, J. D., Zhou, S. Z., He, Y. Q., Ye, Y. G., and Liu, S. Y. (2006). ESR dating of glacial tills and glaciations in the Urumqi River headwaters, Tianshan Mountains, China. *Quaternary International* **144**, 61-67.

Conference Announcement

UK Luminescence and ESR Meeting

Department of Geography
University of Liverpool

7-9th September 2006



THE UNIVERSITY
of LIVERPOOL

Please note that the dates for this meeting have changed since the announcement in the previous issue of Ancient TL. The correct dates for the meeting are as given above (7th – 9th September 2006).

The deadline for registration is 1st July, and Final titles abstracts are also required by 1st July. Further information is available at the meeting website <http://www.liv.ac.uk/geography/LUM2006>., or by e-mailing to LUM2006@liv.ac.uk.

